Journal of Materials Chemistry B

PAPER

View Article Online
View Journal

Cite this: DOI: 10.1039/c4tb01713g

Designed self-assembled hybrid Au@CdS core–shell nanoparticles with negative charge and their application as highly selective biosensors

Wuxiang Zhang,[a] Jianzhong Zheng,*[abc] Changhui Tan,[ac] Xuan Lin,[ac] Shirong Hu,[ac] Jianhua Chen,[ac] Xiuli You*[ac] and Shunxing Li[ac]

Received 16th October 2014
Accepted 2nd November 2014

DOI: 10.1039/c4tb01713g

www.rsc.org/MaterialsB

A novel and general strategy for the synthesis of a monodispersed Au@CdS core–shell structure with uniform morphology and size through a self-assembly process is proposed here. The obtained negatively charged Au@CdS hybrid core–shell nanoparticles (NPs) are highly selective to dopamine (DA), in the presence of oxidation of ascorbic acid (AA) and uric acid (UA), based on electrostatic interaction. The fabricated biosensor shows a wide linear range from 0.002 to 800 μmol L^{-1}, with a lower detection limit of 0.55 nmol L^{-1} ($n = 5$, $S/N = 3$), revealing the high-sensitivity properties. Electrostatic charge plays an important role in the selective electrocatalytic activity of Au@CdS hybrid core–shell nanoparticles, that is the formation of an electrostatic system between the negatively charged Au@CdS hybrid core–shell NPs and the DA cation. The modified electrode is used to achieve the real-time quantitative detection of DA for biological applications, and satisfactory results are obtained. Due to the advantages of the biosensor, its selectivity, sensitivity and stability, it will have a bright future in the field of medical diagnosis.

1. Introduction

Functional materials composed of two or more components have received more and more attention, due to the combination of the unique properties of each component, or the new properties achieved due to the synergistic effect.[1–5] Recently, the synthesis of functional materials in the field of biosensors has focussed on their various applications in medical diagnostics and environmental monitoring. Among the various fantastic structures, the core–shell structure is an excellent candidate, not only from the point of view of facility and importance of the synthesis method,[6–9] by tailoring both the properties of the shells and the interior cores,[10,11] but also the properties, such as electronic and catalytic properties relative to a single-component composition.[12–17] Moreover, enhancement in activity,[18–21] selectivity,[22] sensitivity and stability [23,24] are achieved compared to pure metal components, due to the synergistic effects between the metal core and the shell of the semiconductor core–shell nanostructures. Therefore, to date, electrochemical applications based on Au@SiO_2,[25] Au@SnO_2,[26] Ag@Ag_2O,[27] Pt@*meso*-SiO_2,[28] Fe@Fe_2O_3[29] and Ni/NiO[30] have been gradually investigated and applied. Therefore, introducing metal-semiconductor core–shell nanostructured materials into biosensors may pave the way for applications in the fields of biosensors.[24,31–33]

Noble metal nanomaterials fabricated into the core–shell structure have played an important role in hybrid nanomaterials.[34–37] Au nanoparticles (NPs) have been the subject of intense research and various applications are anticipated in sensing,[38–40] catalysis,[41] and imaging.[42,43] Recently, Lee *et al.*[44] have reported the selective determination of DA using quantum-sized gold nanoparticles. Zhao *et al.*[45] have successfully prepared functional Fe_3O_4@Au nanocomposites for hydrolase biosensor design, which showed excellent properties. In the past decade, semiconductor nanoparticles with excellent physicochemical properties have also attracted increasing attention due to their unique size-dependent chemical and physical properties.[46–51] Semiconductor nanocrystals are of great interest.[52,53] Specifically, high-quality CdS nanoparticles are employed to develop sensor[54] and biosensor systems,[55–57] light-emitting diodes,[58] and lasers.[59,60] Zhu and coworkers have developed a novel label-free biosensor of CdS nanoparticles with co-reactant $K_2S_2O_8$ for the detection of low density lipoprotein.[61] Wang and coworkers have demonstrated that the CdS nanoparticles formed on the surface of multi-walled carbon nanotubes can react with the co-reactant of H_2O_2 in a neutral PBS solution.[62]

Dopamine, an important neurotransmitter, has been extensively studied,[63] as it plays an important part in the functions of

[a]College of Chemistry and Environment, Minnan Normal University, Zhangzhou 363000, P.R. China. E-mail: zhengjianzhong49@163.com; youxiuli520@126.com; Fax: +86 596 2591445; Tel: +86 596 2591445

[b]Zhangzhou Environmental Monitoring Station, Zhangzhou 363000, P. R. China

[c]Fujian Provincial Key Laboratory of Modern Analytical Science and Separation Technology, Zhangzhou 363000, P. R. China

the central nervous system and cardiovascular system.[64,65] Worse still, an abnormal dopaminergic neuron process may lead to neurological diseases.[66,67] Therefore, rapid detection of dopamine is very important and meaningful for the analysis and diagnosis of neurological disorders.[68] As to the electroactive properties of DA, electrochemical methods have been proposed as a viable technique for the determination of DA because of its advantages of high sensitivity, and low operating and instrumental expenses.[69–71]

Here we report a novel method for the fabrication of monodispersed core–shell nanostructures with charged sodium citrate stabilizer, composed of a single gold core surrounded by CdS quantum dots (QDs). Sodium citrate protected Au@CdS hybrid core–shell NPs are immobilized on a glassy carbon electrode (GCE) for selective determination of DA in the presence of AA and UA. The method shows stable performance, high sensitivity and low detection limit down to 0.55 nM for DA, which is sensitive for characterizing DA levels in many biological systems. Finally, real samples have also been tested to validate the utility of this sensor toward selective determination of DA.

2. Experimental

2.1. Materials

Typically, $Cd(ClO_4)_2 \cdot 6H_2O$, NaOH, sodium citrate dehydrate and thioacetamide were purchased from Alfa Aesar. $HAuCl_4 \cdot 3H_2O$ was bought from Sinopharm Chemical Reagent Co. Ltd. Phosphate buffer solution (PBS) was from Shanghai Kangyi Instrument Co., Ltd. Dopamine, uric acid and ascorbic acid were obtained from Shanghai Sinopharm Chemical Reagent Co., Ltd. Real samples (human serum and urine) were provided from Zhangzhou hospital. All other reagents are analytical reagents. All chemicals and solvents were used as received. All aqueous solutions were prepared using ultrapure water (18.2 MΩ cm) from a Milli-Q system (Millipore).

2.2. Synthesis of CdS QDs and self-assembly of hybrid Au@CdS core–shell NPs

Synthesis of CdS QDs and self-assembly of hybrid Au@CdS core–shell NPs: for CdS QD preparation, 3.4×10^{-4} mol sodium citrate and 1.6×10^{-4} mol $Cd(ClO_4)_2 \cdot 6H_2O$ were dissolved in 86 mL water, followed by adjusting the pH to the range 7.9–9.5 by 0.5 mol L^{-1} NaOH. The solution was deaerated by nitrogen bubbling for 15 min. Under vigorous stirring, 4.0×10^{-5} mol thioacetamide solution was injected into the above system. Afterwards, the resulting solution mixture was heated to 80 °C and refluxed under flowing nitrogen for 24 h.

CdS QDs assembled around preformed Au NPs formed hybrid Au@CdS core–shell NPs. Spherical Au NPs with average diameter 13 nm were synthesized according to the citrate reduction of $HAuCl_4$.[72,73] The method is briefly depicted as follow: 2.5×10^{-5} mol $HAuCl_4$ was dissolved in 99 mL water, the solution was brought to boil while being stirred, and the corresponding amount of 1 mL 8.75×10^{-5} mol sodium citrate solution was added quickly. The solution was then boiled for an additional 30 min and cooled to room temperature. Subsequently, in order to coat CdS shells on the Au NPs, 40 mL solution containing Au NPs was diluted to 80 mL using water, and 2.0×10^{-5} mol sodium citrate and 9.0×10^{-6} mol $Cd(ClO_4)_2 \cdot 6H_2O$ were added, followed by adjusting the pH to 9.3 by 0.5 mol L^{-1} NaOH. After the mixture solution was deaerated by bubbling argon for 15 min, 3.0×10^{-6} mol thioacetamide (in 1 mL water) was injected under vigorous stirring. The resulting solution was further heated to 70 °C and refluxed under flowing nitrogen for 12 h.

2.3. Characterizations

UV-Vis spectra of aqueous solutions containing CdS supraparticles or Au@CdS core–shell supraparticles were obtained using a Hitachi-U-3010 spectrophotometer at room temperature. The morphologies of the samples were observed by scanning electron microscopy (SEM, Hitachi S-4800, Japan) under an accelerating voltage of 10 kV. Transmission Electron Microscopy (TEM) was conducted on a FEI Tecnai G2 S-TWIN and the accelerating voltage used was 200 kV. Scanning transmission electron microscopy (STEM) and energy dispersive X-ray spectroscopy (EDX) mapping investigations were performed in G2 F20 U-TWIN (FEI, America) using a high-angle annular dark field (HAADF) detector. High-resolution TEM was also performed using a G2 F20 U-TWIN TEM operating at 200 kV. NPs in solution were analyzed for ξ-potential values using dynamic light scattering (Zetasizer Nano ZS series, Malvern Instruments) with 633 nm laser wavelength and a measurement angle of 173° (backscatter detection) at 25 °C. All electrochemical measurements were performed on a CHI650E electrochemical workstation (ChenHua Instruments Co., Shanghai, China). A conventional three-electrode system was employed, with the modified glassy carbon electrode (GCE, 3 mm in diameter) as the working electrode, a saturated Ag/AgCl electrode as the reference electrode and a platinum wire as the auxiliary electrode. The pH measurements were carried out on a PHS-3C type precise pH meter (KangYi Instrument Co., Ltd, Shanghai, China).

2.4. Fabrication of the modified electrode

The glassy carbon electrode (GCE) was polished to a mirror finish with a piece of diamond paper and 0.05 μm alumina slurry sequentially and then cleaned ultrasonically in ethanol and water for 1 min, respectively. The cleaned GCE was dried with nitrogen steam for the next modification. Then 5.0 μL of the Au@CdS core–shell NP dispersion was dropped onto the GCE surface and dried at room temperature. Then the modified electrodes were obtained.

2.5. Electrochemical measurement

Cyclic voltammetry (CV) and differential-pulse voltammetry (DPV) measurements were carried out with a CHI 660E electrochemistry workstation in 0.1 M phosphate buffered saline with a conventional three-electrode system comprising a platinum wire as the auxiliary electrode, a saturated Ag/AgCl

electrode as the reference electrode and the modified GCE as the working electrode.

3. Results and discussion

3.1. Preparation of Au@CdS core–shell NPs and the corresponding characterization

The morphologies and microstructure of the samples were characterized by means of transmission electron microscopy (TEM). Fig. 1a and b illustrate the typical TEM images of Au NPs and CdS supraparticles, respectively. The Au NPs were clearly identifiable and appeared uniform in size with a diameter of ~13 nm. The TEM image (Fig. 1c) clearly shows that all the Au@CdS products having core–shell structures with uniform size 22 nm and shape were successfully synthesized by self-assembly of *in situ* formed CdS NPs. The formation of such monodispersed core–shell nanostructures and supraparticles can be attributed to the balanced van der Waals attraction and electrostatic repulsion between CdS QDs.[74] Results from high-resolution transmission electron microscopy (HRTEM) imaging indicate that the spacing between two adjacent lattice planes is about 0.34 nm and 0.20 nm (Fig. 1d), which is in agreement with the spacing of the (002) and (220) planes of CdS, respectively, indicating that the shells in the core–shell NPs are CdS.

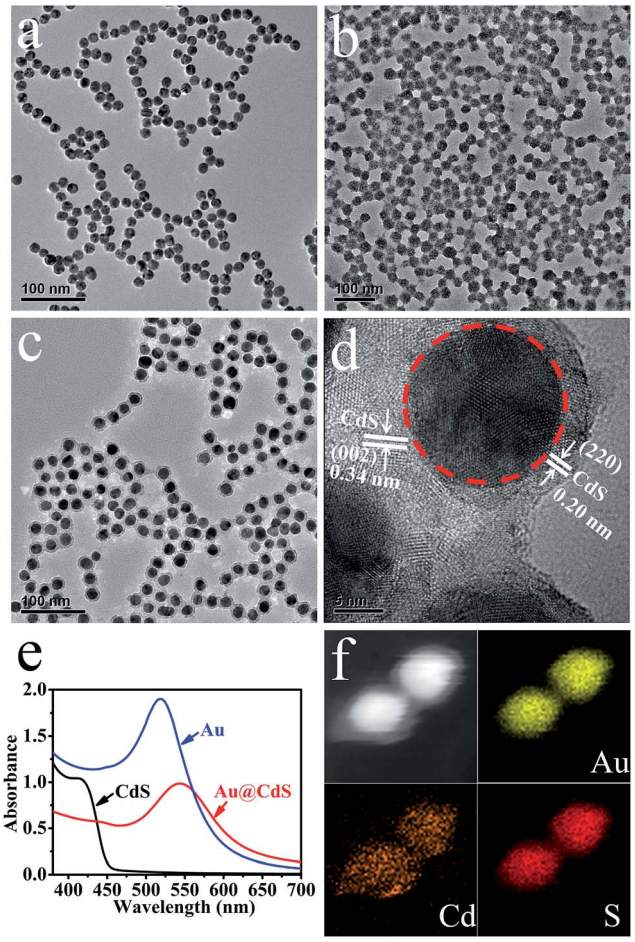

Fig. 1 TEM images of (a) Au NPs, (b) CdS supraparticles and (c) Au@CdS core–shell nanostructures; (d) HRTEM image of a core–shell Au@CdS NP. (e) Ultraviolet-Visible spectra of Au NPs, CdS supraparticles and Au@CdS core–shell nanostructures. (f) HAADF-STEM image of core–shell Au@CdS NPs with a shell and EDX (Energy-dispersive X-ray spectroscopy) elemental mapping of the Au@CdS core–shell nanostructures.

The optical properties of colloidal Au NPs, CdS QDs and Au@CdS core–shell nanostructures suspension solutions are further investigated for confirming monodispersed Au@CdS core–shell NPs by UV-Vis absorption spectra and the results are shown in Fig. 1e. Both the Au NP and Au@CdS core–shell nanostructure suspension solutions display absorption peaks at 519 nm and 544 nm, respectively, which is the characteristic band of well dispersed Au NPs. The small red-shift might result from the interaction between Au NPs and CdS. Furthermore, the composition of the core–shell NPs is studied in high-angle annular dark field scanning transmission electron microscopy (HAADFSTEM) imaging and energy-dispersive X-ray (EDX) elemental mapping (Fig. 1f). The results of the HAADF-STEM image (Fig. 1f) demonstrate that NPs have a typical core–shell structure, and EDX elemental mapping indicates that the element Au is located in the core and that the elements Cd and S of CdS are homogenously distributed throughout the whole NP (Fig. 1f), showing that a Au NP core is surrounded with a uniform CdS shell.

3.2. Electrocatalysis of the Au@CdS core–shell NPs sensor against DA

The electrocatalytic activities of Au@CdS core–shell NPs toward DA, AA and UA have been investigated by cyclic voltammetry (CV), as shown in Fig. 2a and b. In the absence of DA, no obvious peaks were obtained for Au@CdS NPs due to reduction. However, with Au@CdS core–shell NPs, they have been used to modify electrodes along with charged sodium citrate stabilizer for the selective determination of DA in the presence of AA and UA. A possible reaction mechanism was discussed here, as illustrated in Scheme 1. It is well known that Au NPs have high surface energies and tend to aggregate and fuse; as a result the intriguing properties observed for the NPs disappear and difficulties arise for long term storage, processing, and applications. Therefore, great efforts have been devoted to develop novel strategies to stabilize NPs. First, the surrounding CdS QDs not only acted as physical barriers to protect the Au NPs from aggregation and chemical poisoning by offering more reactive sites in the electrochemical reaction, but also act as an electron transfer channel, accelerating the electron transfer between Au NPs and the CdS shell.[75,76] Second, the negatively charged Au@CdS NPs not only act as electrocatalysts, but also serve as selective reagents, which attract positive charge and repel negatively charged analytes such as AA and UA. In other words they are selective for the positively charged DA analyte by electrostatic interaction.[77,78] In conclusion, the combination of the above two factors brings an electrocatalytic synergy to DA. To confirm this assumption, zeta potential measurement of the sample in aqueous solution is carried

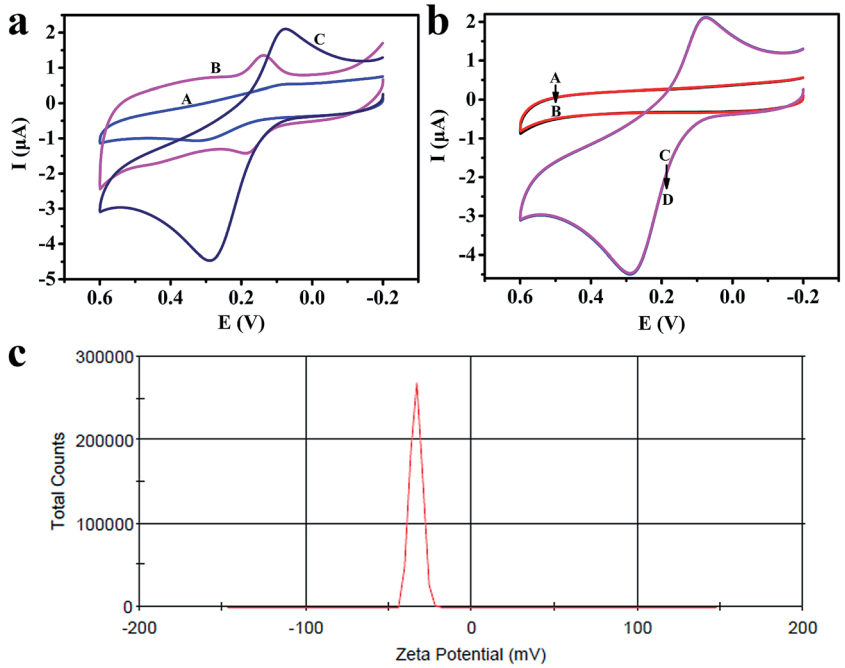

Fig. 2 (a) CV of 0.1 mM DA on CdS supraparticles (A), Au NPs/GCE (B), core–shell Au@CdS NPs/GCE (C) in 0.1 M PBS (pH 7.0) at scan rate 0.1 V s^{-1}. (b) CV demonstrating the electrocatalytic oxidation of DA, AA and UA in 0.1 M PBS (pH 7.0) at scan rate 0.1 V s^{-1}; curves A–D correspond to CV of core–shell Au@CdS NPs in the presence of 0, 0.5 mM AA and 0.5 mM UA, 0.1 mM DA, 0.1 mM DA and (B), respectively. (c) Zeta potential of citrate-capped spherical Au@CdS core–shell NPs.

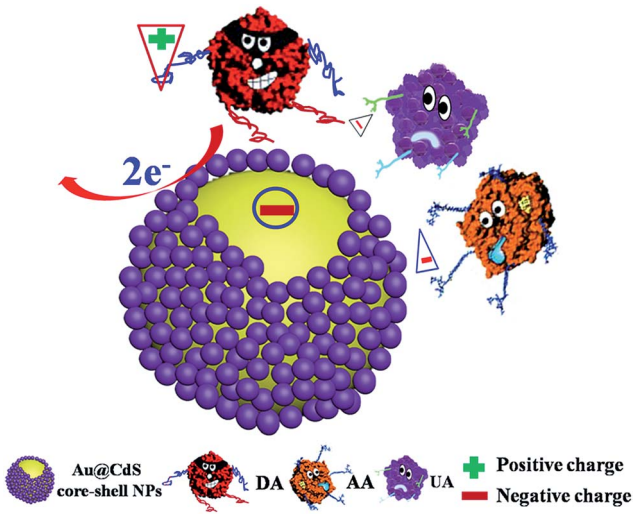

Scheme 1 Schematic illustration of the reaction mechanism of the Au@CdS core–shell structure with DA in the presence of UA and AA.

out. As shown in Fig. 2c, the zeta potential of the citrate-capped spherical Au@CdS core–shell NPs is −33.4 mV. The p*K*a values of DA, UA and AA are 8.9, 3.9 and 4.1, respectively, indicating that DA exists as a cation and UA and AA an anions at neutral pH. The result shown in Fig. 2 therefore suggests that the Au@CdS core–shell NPs could exhibit selective electrocatalytic activity towards DA, based on the electrostatic interaction between negatively charged Au@CdS core–shell NPs and positively charged DA analytes.

3.3. Optimization of the DA biosensor

In this work, pH value and scan rate, which are the important parameters in biosensing, were studied to ascertain the optimal working conditions of the DA biosensor. Since the electrocatalytic reaction at the Au@CdS core–shell NP biosensor is a two electron, two proton process, the pH effect on the biosensor performance was investigated by measuring the electrochemical response in 0.1 M pH 7.00 PBS, with pH values ranging from 4.0 to 9.0. The electrochemical responses increased with pH from 4.0 to 9.0 (Fig. 3a), as high pH can potentially drive the reaction forward more favorably. A good linear relationship between E_{pa} and pH was constructed with a linear regression equation of oxidation peak potentials (E_{pa}) of DA on the Au@CdS core–shell NPs, with a linear equation of $E_{pa}/V = -0.0758$ pH + 0.8265 ($R = 0.9975$) (Fig. 3b). As illustrated in Fig. 3b, a larger response current was obtained within the range of pH 7.0. In addition, as pH 7.0 is close to physiological levels, a phosphate buffer solution of pH 7.0 was chosen and used in all experiments below.

The influence of scan rates (ν) on the electrochemical response of 0.1 mM DA in 0.1 M pH 7.00 PBS at core–shell structured Au@CdS NPs was examined by varying the scan rates from 20 to 700 mV s^{-1} (Fig. 4a). On increasing the scan rate, both anodic and cathodic peak currents increased gradually, yet anodic and cathodic peak potentials slightly shifted to more positive and negative potentials, respectively, generating increased potential separations (ΔE_p). A good linear dependence of redox peak currents on the scan rate was obtained, but

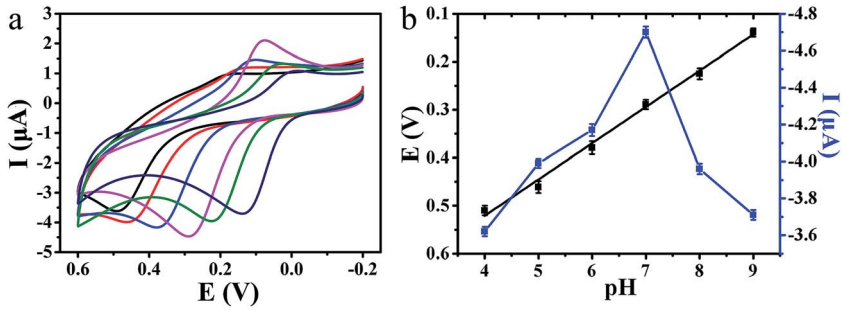

Fig. 3 (a) CV of 0.1 mM DA on the Au@CdS core–shell structure in 0.1 M PBS at different pH of 4.0, 5.0, 6.0, 7.0, 8.0 and 9.0 (from left to right) (scan rate: 0.1 V s^{-1}). (b) The plots of I_{pa} (B) and E_{pa} (A) with pH values.

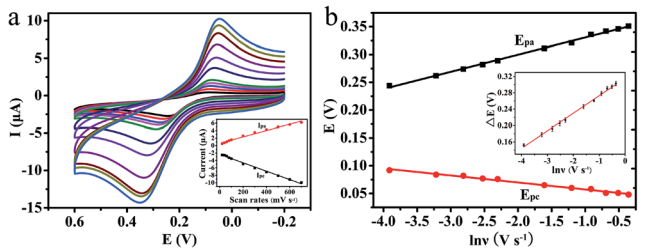

Fig. 4 (a) CV of core–shell Au@CdS NPs in 0.1 mM pH 7.0 PBS containing 0.1 mM DA at different scan rates of 20, 40, 60, 80, 100, 200, 300, 400, 500, 600 and 700 mV s^{-1} (from inside to outside). The inset shows the plots of anodic and cathodic peak currents *vs.* scan rates. (b) The plot of peak potentials (E_p) on the neperian logarithm of scan rates (ln ν), with linear fitting from scan rates 20–700 mV s^{-1}. The inset shows the dependence of peak potential separation (ΔE_p) on ln ν.

without its square root (inset of Fig. 4a); linear regression equations ($R_{pa} = 0.9943$ and $R_{pc} = 0.9967$):

$$I_{pa}\ (\mu A) = 8.44 \times 10^{-3}\ \nu\ (\text{mV s}^{-1}) + 0.6417$$

$$I_{pc}\ (\mu A) = -1.13 \times 10^{-2}\ \nu\ (\text{mV s}^{-1}) - 2.374$$

Integration of the area under anodic peaks led to really close charge values (Q) independent of the scan rate. These results signify that the electrochemical reaction is controlled *via* surface adsorption of DA molecules. As for a quasi-reversible adsorption-controlled process, surface coverage concentration of redox species (G) and the number of electrons (n) can be acquired according to Laviron's equation:

$$I_p = \frac{n^2F^2}{4RT}A\Gamma\nu = \frac{nF}{4RT}Q\nu \quad (1)$$

where A is the electrode surface area, F is Faraday's constant, T is the temperature and R is the ideal gas constant. From Fig. 4a, Q is calculated to be 4.358×10^{-7} C and together with the slope, n is calculated to be 1.99, indicating a two-electron and two-proton process at the sensor interface consistent with the result in the literature.[79] In addition, the relationship between redox peak potentials and ln ν was also built (Fig. 4b) and linear dependence can be found at scan rates from 20 to 700 mV s^{-1}, expressed as:

$$E_{pa}\ (\text{V}) = 0.0308 \times \ln \nu\ (\text{V s}^{-1}) + 0.3615\ (R = 0.9986)$$

$$E_{pc}\ (\text{V}) = -0.0252 \times \ln \nu\ (\text{V s}^{-1}) + 0.0446\ (R = 0.9946)$$

which can be represented by Laviron models:[80,81]

$$E_{pa} = E^{0'} + \frac{RT}{(1-\alpha)\alpha nF}\ln\frac{(1-\alpha)nF}{RTk_s} + \frac{RT}{(1-\alpha)nF}\ln \nu \quad (2)$$

$$E_{pc} = E^{0'} - \frac{RT}{\alpha nF}\ln\frac{\alpha nF}{RTk_s} - \frac{RT}{\alpha nF}\ln \nu \quad (3)$$

Therefore, from the slopes, the electron transfer coefficient α is estimated to be 0.512, close to the theoretical value of 0.5 for a quasi-reversible process. From eqn (2) and (3), the following can be obtained:

$$\Delta E_p = \frac{RT}{(1-\alpha)\alpha nF}\left[\alpha\ln(1-\alpha) + (1-\alpha)\ln\alpha - \ln\frac{RT}{nF} - \ln k_s\right] + \frac{RT}{(1-\alpha)\alpha nF}\ln \nu \quad (4)$$

From the intercept of graph of ΔEp *vs* ln ν (inset of Fig. 4b, $R = 0.9984$), the apparent heterogeneous electron transfer rate constant k_s can be obtained as 1.478 s^{-1}, indicating a fairly fast electron transfer during the electrocatalytic reaction.

3.4. Calibration plot and limit of detection

Voltammetric current responses of successive additions of DA were recorded by differential pulse voltammetry (DPV) to check the sensitivity of the sensor. DPV curves of various concentrations of DA at core–shell structured Au@CdS NPs are shown in Fig. 5. Under optimal conditions, the oxidation peak current (I_{pa}) of DA increased linearly with increasing DA concentration in the range 0.002 μM to 800.0 μM (inset of Fig. 5), with linear regression equations $I_{pa}\ (\mu A) = -0.3967C\ (\mu M) - 17.367$ ($R = 0.9983$). The limit of detection was estimated to be 0.55 nM based on S/N of 3 and the relative standard derivation (RSD, $n = 5$) was less than 2.6%. Furthermore, an important parameter for a biosensor is its ability to discriminate between the interfering species commonly present in similar physiological environments. The influences from common co-existing substances were also investigated, such as NaCl, K_2SO_4 and

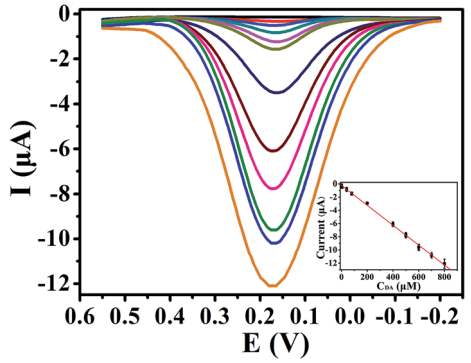

Fig. 5 DPV for different concentrations of DA at Au@CdS hybrid core–shell NPs in 0.1 M PBS with pH 7.0 (scan rate: 0.1 V s^{-1}). The total concentration of DA in each step (from top to bottom: 0, 0.002, 0.1, 1, 20, 30, 200, 400, 500, 600, 700, 800 μM). Inset: the calibration plot of oxidation peak current *vs.* accumulated concentration of DA in each step.

$CaCl_2$ solutions (300 fold), lysine, cysteine, AA, UA and glucose solutions (100 fold). The oxidation peak potential and current of DA showed almost no interference in the presence of any of these influences. In addition, the proposed method has been highlighted by a comparison of the linear range, detection limit and biological applications for Au@CdS hybrid core–shell nanoparticles (NPs) with other dopamine sensors reported in the literature, as shown in Table 1, indicating that the analytical performance for Au@CdS/GCE is comparable and even better than those obtained at several electrodes reported recently. Therefore, the Au@CdS hybrid core–shell NPs are excellent as promising candidates for dopamine sensors with a wide linear range, low detection potential, and high sensitivity.

3.5. Reproducibility and stability of the core–shell structured Au@CdS NPs electrode

The reproducibility and stability of the core–shell structured Au@CdS NP modified electrode were examined. Repeated DPV experiment were run in 5.0×10^{-6} M DA in 0.1 M pH 7.00 PBS. A relative standard deviation (RSD) of about 1.98% after 15 successive measurements was obtained, indicating that the core–shell structured Au@CdS NP modified electrode has excellent reproducibility. The long-term stability of the core–shell structured Au@CdS NP modified electrode was evaluated by measuring its CV response to 5.0×10^{-6} M DA in 0.1 M pH 7.00 PBS and then repeating the same experiment after one month. The electrode was stored at room temperature under normal conditions when not in use. The oxidation current response maintained 97.49% of the original peak current value after one month, indicating good stability of the fabricated electrode.

3.6. Determination of DA in human real samples

To evaluate the potential application of the core–shell structured Au@CdS NP modified electrode, the detection of human real samples was carried out by the standard addition method. The real samples were diluted 5 times with 0.1 M PBS (pH 7.0) before measurement. Then different amounts of known concentrations of DA were added to the sample to obtain the appropriate concentrations. Table 2 represents the results

Table 2 Determination of DA levels in real samples using the Au@CdS hybrid core–shell NPs and DPV in 0.1 M PBS (pH 7.0)

Sample	Detected (μM)	Add (μM)	Found (μM)	Recovery (%)	RSD (%)
Serum 1	0.08	5	5.1 ± 0.5	99.6	2.3
		10	10.1 ± 0.7	101.5	1.9
		15	15.3 ± 1.2	101.2	1.6
Serum 2	0.17	5	5.2 ± 1.4	102.1	2.5
		10	10.3 ± 0.5	100.8	1.4
		15	14.9 ± 1.2	98.6	2.2
Urine 1	0.9	5	4.9 ± 1.8	99.7	2.1
		10	10.4 ± 1.3	100.3	1.9
		15	15.9 ± 1.6	101.4	1.7
Urine 2	1.3	5	5.3 ± 1.0	101.9	2.7
		10	10.4 ± 0.8	98.9	2.3
		15	16.1 ± 1.3	102.9	1.8

Table 1 Comparison of the performance of various dopamine sensors[a]

Author	Electrode materials	Linear range (μM)	Detection limit (nM)	Real-time detection
Teymourian *et al.*[82]	Fe_3O_4/r-GO	0.4–160	80	No
Wang *et al.*[83]	Pd NPs/graphene/chitosan	0.5–200	100	No
Zhang *et al.*[84]	Cu_2O/graphene	0.1–10	10	No
Sun *et al.*[85]	Pt/graphene	0.03–8.13	30	No
Xue *et al.*[86]	Au@polymer	0.02–0.54	7.8	Yes
Mahshid *et al.*[87]	Au/Pt/Pd/TiO_2 NTs	0.05–30	30	Yes
Yang *et al.*[88]	Graphene/SnO_2 NPs	0.1–10	80	Yes
Yu *et al.*[25]	Au@SiO_2–MIPs	0.048–50	20	Yes
Qian *et al.*[89]	Polypyrrole@r-GO	0.06–8	6	No
Li *et al.*[90]	MIPs–OAP–gold	0.02–0.25	1.98	No
Gai *et al.*[91]	N-PCNPs	0.5–30	11	No
This work	Au@CdS NPs	0.002–800	0.55	Yes

[a] Au/Pt/Pd/TiO_2 NTs = Au/Pt/Pd/TiO_2 nanotubes, Au@SiO_2–MIPs = Au@SiO_2–molecularly imprinted polymers, MIPs–OAP–gold = molecularly imprinted polymers–*o*-aminophenol–gold, N-PCNPs = Nitrogen doped porous carbon nanopolyhedra.

obtained for five measurements. The recovery of the spiked samples ranged between 98.6% and 102.9% ($n = 5$), and the relative standard deviation (RSD) values were calculated to be under 2.7%, indicating the potential of the method for detection of DA in real samples.

4. Conclusion

In conclusion, core–shell structured Au@CdS NPs with charge selective stabilizer and uniform morphology/size, in which a single Au nanoparticles core is coated with CdS QDs by an *in situ* self-assembly method, have been prepared. In addition, the proposed hybrid materials have been successfully applied in the detection of dopamine, which exhibited advantages such as efficient detection, sensitivity and good selectivity for dopamine detection in the presence of ascorbic acid and uric acid. A detection limit for dopamine of as low as 0.55 nM was obtained. Furthermore, the proposed method was applied to the determination of DA in real samples with satisfactory results, which could have a bright future in the field of biological applications. This work demonstrated that a charge selective electrochemical sensor could be developed based on core–shell structured Au@CdS NPs protected with a charge selective stabilizer and have a bright future in the field of developing highly selective electrochemical sensors for specific samples.

Acknowledgements

This work was supported by the National Natural Science Foundation of China (no. 21175115 and 21475055 S.X.L), the Program for New Century Excellent Talents in University (NCET-110904), the science and technology program Fujuan Educational Bureau (JA12218), the Program for New Century Excellent Talents in Minnan Normal University (SX1101) and the Fujian Province Undergraduate Innovative Training Program (No. 201410402028 and 201410402029).

References

1 B. Jang, J. Y. Park, C. H. Tung, I. H. Kim and Y. Choi, *ACS Nano*, 2011, **5**, 1086.
2 A. Kyrsting, P. M. Bendix, D. G. Stamou and L. B. Oddershede, *Nano Lett.*, 2011, **11**, 888.
3 W. Wu, J. Shen, P. Banerjee and S. Zhou, *Adv. Funct. Mater.*, 2011, **21**, 2830.
4 Y. Jin, C. Jia, S. W. Huang, M. O. Donnell and X. Gao, *Nat. Commun.*, 2010, **1**, 41.
5 H. Park, J. Yang, J. Lee, S. Haam, I. H. Choi and K. H. Yoo, *ACS Nano*, 2009, **3**, 2919.
6 S. H. Joo, J. Y. Park, C. Tsung, Y. Yamada, P. Yang and G. A. Somorjai, *Nat. Mater.*, 2009, **8**, 126.
7 S. Wu, J. Dzubiella, J. Kaiser, M. Drechsler, X. Guo, M. Ballauff and Y. Lu, *Angew. Chem., Int. Ed.*, 2012, **51**, 2229.
8 C. Kuo, Y. Tang, L. Chou, B. Sneed, C. N. Brodsky, Z. Zhao and C. Tsung, *J. Am. Chem. Soc.*, 2012, **134**, 14345.
9 S. X. Li, J. Z. Zheng, D. J. Chen, Y. J. Wu, W. X. Zhang, F. Y. Zheng, J. Cao and Y. L. Liu, *Nanoscale*, 2013, **5**, 11718.
10 Q. Zhang, I. Lee, J. B. Joo, F. Zaera and Y. Yin, *Acc. Chem. Res.*, 2013, **46**, 1816.
11 W. Li, Y. Deng, Z. Wu, X. Qian, J. Yang, Y. Wang, D. Gu, F. Zhang, B. Tu and D. Zhao, *J. Am. Chem. Soc.*, 2011, **133**, 15830.
12 M. B. Cortie and A. M. McDonagh, *Chem. Rev.*, 2011, **111**, 3713.
13 M. Sastry, A. Swami, S. Mandal and P. R. Selvakannan, *J. Mater. Chem.*, 2005, **15**, 3161.
14 A. Burns, H. Ow and U. Wiesner, *Chem. Soc. Rev.*, 2006, **35**, 1028.
15 H. Ataee-Esfahani, L. Wang and Y. Yamauchi, *Chem. Commun.*, 2010, **46**, 3684.
16 F. Tao, M. E. Grass, Y. Zhang, D. R. Butcher, J. R. Renzas, Z. Liu, J. Y. Chung, B. S. Mun, M. Salmeron and G. A. Somorjai, *Science*, 2008, **322**, 932.
17 K. Zhang, Y. J. Xiang, Z. C. Wu, L. L. Feng, W. W. He, J. B. Liu, W. Y. Zhou and S. S. Xie, *Langmuir*, 2009, **25**, 1162.
18 M. Chen, D. Kumar, C. W. Yi and D. W. Goodman, *Science*, 2005, **310**, 291.
19 L. Kuai, S. Z. Wang and B. Y. Geng, *Chem. Commun.*, 2011, **47**, 6093.
20 C. H. Cui, J. W. Yu, H. H. Li, M. R. Gao, H. W. Liang and S. H. Yu, *ACS Nano*, 2011, **5**, 4211.
21 S. J. Guo, J. Li, S. J. Dong and E. Wang, *J. Phys. Chem. C*, 2010, **114**, 15337.
22 S. Zhou, K. Mcllwrath, G. Jackson and B. Eichhorn, *J. Am. Chem. Soc.*, 2006, **128**, 1780.
23 A. Cao and G. Veser, *Nat. Mater.*, 2010, **9**, 75.
24 X. Q. Huang, S. H. Tang, B. J. Liu, B. Ren and N. F. Zheng, *Adv. Mater.*, 2011, **23**, 3420.
25 D. J. Yu, Y. B. Zeng, Y. X. Qi, T. S. Zhou and G. Y. Shi, *Biosens. Bioelectron.*, 2012, **38**, 270.
26 Q. M. Shen, J. Y. Jiang, S. L. Liu, L. Han, X. H. Fan, M. X. Fan, Q. L. Fan, L. H. Wang and W. Huang, *Nanoscale*, 2014, **6**, 6315.
27 J. Ghilane, F. R. F. Fan and A. J. Bard, *Nano Lett.*, 2007, **7**, 1406.
28 Z. X. Li, M. C. Liu, L. F. Fan, H. Y. Ke, C. F. Luo and G. H. Zhao, *Biosens. Bioelectron.*, 2014, **52**, 293.
29 X. L. Wang, T. Yang and K. Jiao, *Biosens. Bioelectron.*, 2009, **25**, 668.
30 X. F. Li, A. Dhanabalan, K. Bechtold and C. L. Wang, *Electrochem. Commun.*, 2010, **12**, 1222.
31 B. Khlebtsov, E. Panfilova, V. Khanadeev, O. Bibikova, G. Terentyuk, A. Ivanov, V. Rumyantseva, I. Shilov, A. Ryabova, V. Loshchenov and N. G. Khlebtsov, *ACS Nano*, 2011, **5**, 7077.
32 J. Yang, J. Choi, D. Bang, E. Kim, E. K. Lim, H. Park, J. S. Suh, K. Lee, K. H. Yoo, E. K. Kim, Y. M. Huh and S. Haam, *Angew. Chem.*, 2011, **123**, 461.
33 J. Yang, J. Choi, D. Bang, E. Kim, E. K. Lim, H. Park, J. S. Suh, K. Lee, K. H. Yoo, E. K. Kim, Y. M. Huh and S. Haam, *Angew. Chem., Int. Ed.*, 2011, **50**, 441.
34 X. Huang, S. Tang, B. Liu, B. Ren and N. Zheng, *Adv. Mater.*, 2011, **23**, 3420.

35 H. Liu, D. Chen, L. Li, T. Liu, L. Tan, X. Wu and F. Tang, *Angew. Chem.*, 2011, **123**, 921.
36 H. Liu, D. Chen, L. Li, T. Liu, L. Tan, X. Wu and F. Tang, *Angew. Chem., Int. Ed.*, 2011, **50**, 891.
37 W. Wu, J. Shen, P. Banerjee and S. Zhou, *Biomaterials*, 2010, **31**, 7555.
38 J. N. Anker, W. P. Hall, O. Lyandres, N. C. Shah, J. Zhao and R. P. Van Duyne, *Nat. Mater.*, 2008, **7**, 442.
39 C. Gao, Z. Lu, Y. Liu, Q. Zhang, M. Chi, Q. Cheng and Y. Yin, *Angew. Chem.*, 2012, **124**, 5727.
40 C. Gao, Z. Lu, Y. Liu, Q. Zhang, M. Chi, Q. Cheng and Y. Yin, *Angew. Chem., Int. Ed.*, 2012, **51**, 5629.
41 C. Burda, X. Chen, R. Narayanan and M. A. El-Sayed, *Chem. Rev.*, 2005, **105**, 1025.
42 N. J. Durr, T. Larson, D. K. Smith, B. A. Korgel, K. Sokolov and A. Ben-Yakar, *Nano Lett.*, 2007, **7**, 941.
43 C. J. Murphy, A. M. Gole, S. E. Hunyadi, J. W. Stone, P. N. Sisco, A. Alkilany, B. E. Kinard and P. Hankins, *Chem. Commun.*, 2008, 544.
44 K. Kwak, S. Senthil Kumar and D. Lee, *Nanoscale*, 2012, **4**, 4240.
45 Y. T. Zhao, W. Y. Zhang, Y. H. Lin and D. Du, *Nanoscale*, 2013, **5**, 1121.
46 M. L. Steigerwald and L. E. Brus, *Acc. Chem. Res.*, 1990, **23**, 183.
47 A. P. Alivisatos, *Science*, 1996, **271**, 933.
48 H. Weller, *Angew. Chem. Int. Ed.*, 1993, **32**, 41.
49 H. Weller, *Curr. Opin. Colloid Interface Sci.*, 1998, **3**, 194.
50 A. Eychmüller, *J. Phys. Chem. B*, 2000, **104**, 6514.
51 M. Green and P. O'Brien, *Chem. Commun.*, 1999, 2235.
52 Reviews relevant to colloidal nanocrystals, *Acc. Chem. Res.*, 1999, **32**, 387, Special Issue for Nanostructures.
53 A. P. Alivisatos, *Science*, 1996, **271**, 933.
54 T. W. Kim, D. U. Lee and Y. S. Yoon, *J. Appl. Phys.*, 2000, **88**, 3759.
55 M. Bruchez Jr, M. Moronne, P. Gin, S. Weiss and A. P. Alivisatos, *Science*, 1998, **281**, 2013.
56 W. C. W. Chan and S. Nie, *Science*, 1998, **281**, 2016.
57 I. Willner, F. Patolsky and J. Wasserman, *Angew. Chem., Int. Ed.*, 2001, **40**, 1861.
58 N. Tessler, V. Medvedev, M. Kazes, S. Kan and U. Banin, *Science*, 2002, **295**, 1506.
59 L. Pavesi, L. D. Negro, C. Mazzoleni, G. Franzo and F. Priolo, *Nature*, 2000, **408**, 440.
60 A. V. Malko, A. A. Mikhailovsky, M. A. Petruska, J. A. Hollingsworth, H. Htoon, M. G. Bawendi and V. I. Klimov, *Appl. Phys. Lett.*, 2002, **81**, 1303.
61 G. F. Jie, B. Liu, H. C. Pan, J. J. Zhu and H. Y. Chen, *Anal. Chem.*, 2007, **79**, 5574.
62 X. F. Wang, Y. Zhou, J. J. Xu and H. Y. Chen, *Adv. Funct. Mater.*, 2009, **19**, 1444.
63 R. M. Wightman, J. A. Jankowski, R. T. Kennedy, K. T. Kawagoe, T. J. Schroeder, D. J. Leszczyszyn, J. A. Neart, E. J. Diliberto and O. H. Viveros, *Proc. Natl. Acad. Sci. U. S. A.*, 1991, **88**, 10754.
64 S. Ikemoto, *Brain Res. Rev.*, 2007, **56**, 27.
65 J. R. Wickens, J. C. Horvitz, R. M. Costa and S. J. Killcross, *J. Neurosci.*, 2007, **27**, 8181.
66 T. S. Tang, X. Chen, J. Liu and I. J. Bezprozvanny, *J. Neurosci.*, 2007, **27**, 7899.
67 T. S. Tang, X. Chen, J. Liu, I. J. Bezprozvanny and J. E. Ahlskog, *Neurology*, 2007, **69**, 1701.
68 S. R. Laviolette, *Schizophr. Bull.*, 2007, **33**, 971.
69 G. Fabregat, E. C. Ordova-Mateo, E. Armelin, O. Bertran and C. Aleman, *J. Phys. Chem. C*, 2011, **115**, 14933.
70 N. F. Atta, A. Galal and R. A. Ahmed, *Bioelectrochemistry*, 2011, **80**, 132.
71 R. B. Keithley, P. Takmakov, E. S. Bucher, A. M. Belle, C. A. Owesson-White, J. Park and R. M. Wightman, *Anal. Chem.*, 2011, **83**, 3563.
72 J. Turkevich, P. C. Stevenson and J. S. Hillier, *Discuss. Faraday Soc.*, 1951, **11**, 55.
73 X. Ji, X. Song, J. Li, Y. Bai and W. P. X. Yang, *J. Am. Chem. Soc.*, 2007, **129**, 13939.
74 Y. S. Xia, T. D. Nguyen, M. Yang, B. Lee, A. Santos, P. Podsiadlo, Z. Y. Tang, S. C. Glotzer and N. A. Kotov, *Nat. Nanotechnol.*, 2012, **6**, 580.
75 L. Jia, D. H. Wang, Y. X. Huang, A. W. Xu and H. Q. Yu, *J. Phys. Chem. C*, 2011, **115**, 11466.
76 A. D. Quach, G. Crivat, M. A. Tarr and Z. Rosenzweig, *J. Am. Chem. Soc.*, 2011, **113**, 2028.
77 J. B. Raoof, A. Kiani, R. Ojani, R. Valiollahi and S. Rashid-Nadimi, *J. Solid State Electrochem.*, 2009, **14**, 1171.
78 C. R. Raj, T. Okajima and T. Ohsaka, *J. Electroanal. Chem.*, 2003, **543**, 127.
79 J. Yang, J. R. Strickler and S. Gunasekaran, *Nanoscale*, 2012, **4**, 4594.
80 E. Laviron, *J. Electroanal. Chem.*, 1974, **52**, 355.
81 E. Laviron, *J. Electroanal. Chem.*, 1979, **101**, 19.
82 H. Teymourian, A. Salimi and S. Khezrian, *Biosens. Bioelectron.*, 2013, **49**, 1.
83 X. Wang, M. Wu, W. Tang, Y. Zhu, L. W. Wang, Q. J. Wang, P. J. He and Y. Z. Fang, *J. Electroanal. Chem.*, 2013, **695**, 10.
84 F. Y. Zhang, Y. J. Li, Y. E. Gu, Z. H. Wang, Z. H. Wang and C. M. Wang, *Microchim. Acta*, 2011, **173**, 103.
85 C. L. Sun, H. H. Lee, J. M. Yang and C. C. Wu, *Biosens. Bioelectron.*, 2011, **26**, 3450.
86 C. Xue, Q. Han, Y. Wang, J. H. Wu, T. T. Wen, R. Y. Wang, J. L. Hong, X. M. Zhou and H. J. Jiang, *Biosens. Bioelectron.*, 2013, **49**, 199.
87 S. Mahshid, C. C. Li, S. S. Mahshid, M. Askari, A. Dolati, L. X. Yang, S. L. Luo and Q. Y. Cai, *Nanoscale*, 2011, **136**, 2322.
88 A. K. Yang, Y. Xue, Y. Zhang, X. F. Zhang, H. Zhao, X. J. Li, Y. J. He and Z. B. Yuan, *J. Mater. Chem. B*, 2013, **1**, 1804.
89 T. Qian, S. S. Wu and J. Shen, *Chem. Commun.*, 2013, **49**, 4610.
90 J. P. Li, J. Zhao and X. P. Wei, *Sens. Actuators B: Chemical*, 2009, **140**, 663.
91 P. B. Gai, H. J. Zhang, Y. S. Zhang, W. Liu, G. B. Zhu, X. H. Zhang and J. H. Chen, *J. Mater. Chem. B*, 2013, **1**, 2742.

